DALTON
FULL PAPER

Influences of secondary metal–ligand subunits on molybdenum oxide structures: the hydrothermal syntheses and structures of $[M(tpytrz)_2Mo_4O_{13}]$ (M = Fe, Co, Ni, Zn; tpytrz = tripyridyltriazine), $[Ni(tpytrz)Mo_2O_7]$ and $[Zn_2(tpytrz)Mo_2O_8]$

Randy S. Rarig, Jr. and Jon Zubieta *

Department of Chemistry, Syracuse University, Syracuse, NY 13244, USA

Received 5th June 2001, Accepted 28th September 2001
First published as an Advance Article on the web 9th November 2001

The hydrothermal reactions of the appropriate salts of the first row transition metal dipositive cations M′(II), MoO_3 and 2,4,6-tri(4-pyridyl)-1,3,5-triazine (tpytrz) yielded the bimetallic oxide hybrid solids $[M'(tpytrz)_2Mo_4O_{13}]$ [M′ = Fe (**1**), Co (**2**), Ni (**3**), Zn (**4**)], $[Ni(tpytrz)Mo_2O_7]$ (**6**) and $[Zn_2(tpytrz)Mo_2O_8]$ (**7**) and the molecular compound $[Ni(H_2O)_4(Htpytrz)_2][Mo_8O_{26}]\cdot 1.2H_2O$ (**5**·$1.2H_2O$). The isomorphous series **1**–**4** exhibits a two-dimensional bimetallic oxide network constructed from chains of corner-sharing Mo(VI) octahedra and tetrahedra, linked by $\{M'O_4N_2\}$ octahedra. The inorganic layers are tethered by bidentate tpytrz ligands, each of which bonds to an M′ site of one layer and an octahedral $\{MoO_5N\}$ site of an adjacent layer, with one pyridyl group adopting a pendant mode in the interlamellar region. In contrast, the structure of $[Ni(tpytrz)Mo_2O_7]$ (**6**), while adopting the prototypical motif of alternating bimetallic oxide networks and bridging ligand domains, is characterized by an oxide layer constructed from bimolybdate units $\{Mo_2O_7\}^{2-}$ linked through $\{NiO_4N_2\}$ octahedra. Curiously, the $\{Zn_2Mo_2O_8\}$ network of $[Zn_2(tpytrz)Mo_2O_8]$ (**7**) is constructed from $\{MoO_4\}$ tetrahedra linked through binuclear units of edge-sharing $\{ZnO_4N\}$ square pyramids.

The metal oxides are a ubiquitous family of materials exhibiting a diverse compositional range and considerable structural versatility,[1,2] as well as possessing useful electronic, magnetic, optical, and mechanical properties for the design of novel functional materials. One approach to the synthesis of more complex oxide materials is to introduce organic or metal–organic building blocks to provide additional structural diversity and control of the resultant architecture.[3–5] Such hybrid organic–inorganic composites combine the unique characteristics of both components in new solid state materials manifesting or enhancing the properties of the subunits. The structure-directing role of organic molecules has been extensively documented for zeolites,[6] mesoporous compounds of the MCM-41 class,[7] and transition metal phosphates and phosphonates.[8–10]

In addition to serving as charge-compensating and space-filling structural subunits, the organic component may be introduced as a ligand, tethered directly to the metal oxide substructure or to a secondary metal site. We have recently described the structural influences of organonitrogen ligands on molybdenum and vanadium oxides, including $[MoO_3(4,4'\text{-bipyridine})_{0.5}]$, $[MoO_3(\text{triazolate})_{0.5}]$, and $[V_9O_{22}(\text{terpyridine})_3]$.[11,12] An alternative approach exploits the principles of fundamental coordination chemistry to modify the oxide structure. In this case, the organic is introduced as a ligand to a secondary metal site, which is in turn directly coordinated through bridging oxo-groups to the oxide substructure. Consequently, the overall structure reflects both the geometric constraints of the ligand, as manifested in the size, shape, and relative disposition of the donor groups, and the coordination preferences of the secondary metal site, as reflected in the coordination number and geometry, degree of aggregation into oligomeric units and, mode of attachment to the primary metal oxide subunit.

We have exploited this strategy in the development of the structural chemistries of two families of materials: the vanadium oxides of the type V/O/M′/ligand[13–19] and the molybdenum oxides of general form Mo/O/M′/ligand.[20–36] Although the first member of the vanadium oxide family was reported as recently as 1993[37] and systematic studies were only initiated in 1996,[13] there are now some thirty examples of this structure type.[38] Investigations of the molybdenum oxide based materials are similarly in their infancy. However, two distinct subgroups of the Mo/O/M′/L family of materials have emerged. In the first, the molybdenum oxide and the secondary metal–organonitrogen subunit are present as distinct anionic and cationic substructures, respectively.[20–27] In the second class of materials, the secondary metal is incorporated through bridging oxo-groups into the oxide scaffolding as part of a bimetallic oxide.[30–36] As part of our continuing investigations of this latter subclass of molybdenum oxides, we have prepared a series of materials incorporating divalent first row transition metals as the secondary metal and 2,4,6-tri-4-pyridyl-1,3,5-triazine (tpytrz) as the ligand: an isomorphous set of three-dimensional oxides $[M'(tpytrz)_2Mo_4O_{13}]$ [M′ = Fe (**1**), Co (**2**), Ni (**3**), and Zn (**4**)], the molecular $[Ni(H_2O)_4(Htpytrz)_2][Mo_8O_{26}]\cdot 1.2H_2O$ (**5**·$1.2H_2O$), and the framework materials $[Ni(tpytrz)Mo_2O_7]$ (**6**) and $[Zn_2(tpytrz)Mo_2O_8]$ (**7**).

Experimental

Syntheses and spectroscopy

Syntheses were carried out in Parr acid digestion bombs with 23 ml poly(tetrafluoroethylene) liners. All starting materials, with the exception of 2,4,6-tri(4-pyridyl)-1,3,5-trazine, were purchased from Aldrich and used without further purification. 2,4,6-Tri(4-pyridyl)-1,3,5-triazine was prepared according to the literature method.[39] Water was distilled above 0.3 MΩ in-house using a Barnstead model 525 Biopure distilled water center. Infrared spectra were obtained on a Perkin-Elmer 1600 series FTIR spectrometer.

 DOI: 10.1039/b104965h

Preparation of [Fe(tpytrz)$_2$Mo$_4$O$_{14}$] (1). A solution of $FeSO_4 \cdot 7H_2O$ (0.089 g, 0.32 mmol), MoO_3 (0.044 g, 0.306 mmol), 2,4,6-tri(4-pyridyl)-1,3,5-triazine (0.05 g, 0.16 mmol), and 10 ml H_2O (10 g, 555 mmol) in the molar ratio 2 : 1.9 : 2.1 : 3470 was heated at 180 °C for 48 h in a Parr acid digestion bomb after adjustment of pH to *ca.* 8.5 by addition of 20% tetraethylammonium hydroxide. Large orange crystals of **1** were obtained in 35% yield. IR (KBr pellet, cm^{-1}): 1575(s), 1519(s), 1370(s), 1056(s), 955(s), 911(s), 814(s), 652(s).

Preparations of [Co(tpytrz)$_2$Mo$_2$O$_{14}$] (2), [Ni(tpytrz)$_2$Mo$_4$O$_{14}$] (3), [Zn(tpytrz)$_2$Mo$_4$O$_{14}$] (4), [Ni(H$_2$O)$_4$(Htpytrz)$_2$][Mo$_8$O$_{26}$]·1.2H$_2$O (5·1.2H$_2$O), [Ni(tpytrz)Mo$_2$O$_7$] (6), and [Zn$_2$(tpytrz)-Mo$_2$O$_8$] (7). Compounds **2**, **3**, **5**, and **7** were prepared under conditions identical to those employed for **1**, except for the identity of the secondary metal precursor: $Co(NO_3) \cdot 6H_2O$ (**2**), $NiCl_2 \cdot 6H_2O$ (**3**), $NiNO_3 \cdot 6H_2O$ (**5**), and $ZnNO_3 \cdot 6H_2O$ (**7**). Compounds **4** and **6** were synthesized under conditions similar to those for **7** and **3** except that no base was added to adjust the pH. Yields (color): **2**, 75% (orange), **3**, 40% (orange); **4**, 45% (colorless); **5**, 40% (orange); **6**, 75% (green), **7**, 45% (orange). IR (KBr pellet, cm^{-1}): **2**, 1576(s), 1518(s), 1369(s), 1056(s), 958(s), 916(s), 814(2), 653(s). **3**, 1575(s), 1518(s), 1374(s), 1057(s), 917(s), 839(s). **4**, 1575(s), 1518(s), 1378(s), 1057(s), 954(s), 815(s). **5**, 1615(s), 1576(s), 1519(s), 1062(s), 953(s), 922(s), 810(s). **6**, 1654(s), 1522(s), 1373(s), 923(s), 887(s). **7**, 1522(m), 1374(s), 940(s), 903(m), 841(m), 805(m), 777(m).

X-Ray crystallography

Crystallographic data for all compounds were collected with a Bruker P4 diffractometer equipped with a SMART CCD system[40] and using Mo-Kα radiation ($\lambda = 0.71073$ Å). The data were collected at 90 K and corrected for Lorentz and polarization effects.[41] Absorption corrections were made using SADABS.[42] The structure solution and refinement were carried out using the SHELXTL[43] crystallographic software package. The structures were solved using direct methods, and all of the non-hydrogen atoms were located from the initial solution. After locating all of the non-hydrogen atoms in each structure, the model was refined against F^2, initially using isotropic then anisotropic thermal displacement parameters, until the final value of Δ/σ_{max} was less than 0.001. Crystal data for **1**–**7** are summarized in Table 1. Selected bond lengths and angles for compounds **1**–**4** are collected in Table 2. The metrical parameters for **5**, **6**, and **7** are given in Tables 3–5, respectively.

CCDC reference numbers 163168–163174.

See http://www.rsc.org/suppdata/dt/b1/b104965h/ for crystallographic data in CIF or other electronic format.

Results and discussion

The synthetic strategy exploits hydrothermal conditions which favor the isolation of metastable phases, rather than dense phase thermodynamic products, while avoiding thermal decomposition of the organic component.[44–46] Furthermore, the differential solubilities of the organic and inorganic starting materials are not a significant issue under these conditions. In this fashion, the hydrothermal reactions of the appropriate M(II) precursors with MoO_3 and 2,4,6-tri(4-pyridyl)-1,3,5-triazine (tpytrz), at a pH of *ca.* 8.5 (adjusted by the addition of Et_4NOH), yielded the series of compounds of general type [M′(tpytrz)$_2$Mo$_4$O$_{13}$] [M′ = Fe (**1**), Co (**2**), and Ni (**3**)].

However, the critical dependence of compound composition and structure on the temperature and pH of the reaction medium are well documented.[47] Consequently, the reaction of a Ni(II) salt with MoO_3 and tpytrz at pH 8.5, but at 180 °C, rather than 120 °C, yields a second Mo/O/Ni/tpytrz material, the molecular [Ni(H$_2$O)$_4$(Htpytrz)$_2$][Mo$_8$O$_{26}$]·1.2H$_2$O (**5**·1.2H$_2$O). Similarly, the reaction of $NiCl_2 \cdot 6H_2O$ with MoO_3 and tpytrz in the absence of base (pH 7.0) produced [Ni(tpytrz)Mo$_2$O$_7$] (**6**). In the Zn(II) chemistry, [Zn(tpytrz)$_2$Mo$_4$O$_{13}$] (**4**), the fourth member of the [M′(tpytrz)$_2$Mo$_4$O$_{13}$] family, was isolated at a pH of *ca.* 7.0, while [Zn$_2$(tpytrz)Mo$_2$O$_8$] (**7**) is isolated at pH 8.5.

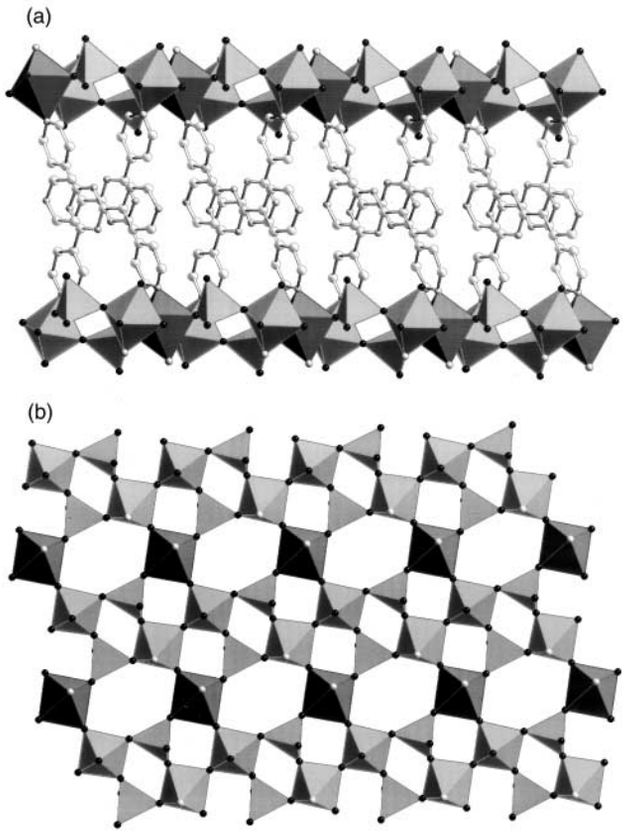

Fig. 1 (a) A polyhedral and ball and stick representation of the framework structure of [Co(tpytrz)$_2$Mo$_4$O$_{13}$] (**2**), showing the organonitrogen ligands bridging the bimetallic oxide networks. (b) A polyhedral representation of the bimetallic oxide network. The color scheme adopted for this figure has been used throughout: Mo, light gray polyhedra; oxygen, small dark gray spheres; carbon, large light gray spheres; nitrogen, small light gray spheres; Co, Ni, and Zn sites are shown as dark gray polyhedra.

The infrared spectra of **1**–**7** exhibited strong bands in the 800 to 960 cm^{-1} range, attributed to ν(Mo=O) and ν(M–O=Mo) [M = Mo or M′(II)]. A group of four peaks in the 1000 to 1580 cm^{-1} region is characteristic of the tpytrz ligand.

As shown in Fig. 1(a) for [Co(tpytrz)$_2$Mo$_4$O$_{13}$] (**3**), the structures of the isomorphous materials **1**–**4** consist of {M′Mo$_4$O$_{13}$} bimetallic oxide layers buttressed by the interlamellar tpytrz ligands. This alternation of inorganic and organic domains, or, alternatively, the sandwiching of organic components between inorganic oxide layers, is a common structural motif in the chemistry of inorganic solids, most notably metal organophosphonate[48] and organic–inorganic perovskite materials.[49]

The oxide layers, shown in Fig. 1b, are constructed from corner-sharing {Co(II)O$_4$N$_2$} octahedra and Mo(VI) octahedra and tetrahedra. The six-coordinate geometry at the M′(II) site is defined by four oxo-groups, one from each of four adjacent Mo polyhedra and two nitrogen donors from each of two tpytrz ligands, occupying *trans* coordination sites.

The molybdenum oxide substructure consists of ribbons of corner-sharing {MoO$_4$} tetrahedra and {MoO$_5$N} octahedra. Within a molybdate ribbon, binuclear units of corner-sharing octahedra are linked to similar neighboring bioctahedral motifs through pairs of tetrahedra. The cobalt sites provide the connectivity between molybdate ribbons to generate the two-dimensional {CoMo$_4$O$_{13}$} oxide substructure. Each Co(II) center bonds to bridging oxo-groups from an octahedral and a

Table 1 Summary of crystallographic data for the structures of $[Fe(tpytrz)_2Mo_4O_{13}]$ (**1**), $[Co(tpytrz)_2Mo_4O_{13}]$ (**2**), $[Ni(tpytrz)_2Mo_4O_{13}]$ (**3**), $[Zn(tpytrz)_2Mo_4O_{13}]$ (**4**), $[Ni(H_2O)_4(Htpytrz)_2][Mo_8O_{26}]\cdot 1.2H_2O$ (**5**·$1.2H_2O$), $[Ni(tpytrz)Mo_2O_7]$ (**6**), and $[Zn_2(tpytrz)Mo_2O_8]$ (**7**)

	1	**2**	**3**	**4**	**5**	**6**	**7**
Empirical formula	$C_{18}H_{12}Fe_{0.50}Mo_2N_6O_{6.50}$	$C_{18}H_{12}Co_{0.50}Mo_2N_6O_{6.50}$	$C_{18}H_{12}Ni_{0.50}Mo_2N_6O_{6.50}$	$C_{18}H_{12}Zn_{0.50}Mo_2N_6O_{6.50}$	$C_{18}H_{18.2}N_6Ni_{0.5}Mo_4O_{15.6}$	$C_{18}H_{12}N_6NiMo_2O_7$	$C_{18}H_{12}Mo_2N_6O_8Zn_2$
Fw	636.14	637.68	637.57	640.9	981.30	674.93	762.96
Cryst. syst.	Triclinic	Triclinic	Triclinic	Triclinic	Monoclinic	Orthorhombic	Orthorhombic
Space group	*P*1	*P*1	*P*1	*P*1	*C*2/*c*	*Pnma*	*Pnma*
a/Å	8.0932(7)	8.068(1)	8.0747(4)	8.0888(6)	28.0815(1)	8.5934(5)	7.0350(6)
b/Å	8.8946(8)	8.881(1)	8.8350(4)	8.9531(7)	13.7086(7)	26.861(1)	30.007(3)
c/Å	13.755(1)	13.698(1)	13.7011(7)	13.680(1)	15.7078(8)	9.1687(5)	10.3080(9)
α/°	79.873(2)	79.885(2)	79.959(1)	79.711(2)	—	—	—
β/°	84.699(2)	84.593(2)	84.275(1)	84.193(1)	111.345(1)	—	—
λ/°	80.517(2)	80.606(2)	80.583(1)	80.275(2)	—	—	—
V/Å^3	959.3(1)	951.2(2)	946.94(8)	958.2(1)	5632.1(5)	2116.9(2)	2176.0(3)
Z	2	2	2	2	8	4	4
D_{calc}/g cm^{-3}	2.202	2.226	2.236	2.221	2.315	2.118	2.329
μ/cm^{-1}	17.28	17.97	18.65	24.75	21.49	21.03	33.66
λ/Mo-K*α*	0.7103	0.7103	0.7103	0.7103	0.7103	0.7103	0.7103
*R*1 [a]	0.0626	0.0692	0.045	0.0952	0.0414	0.0476	0.0695
*wR*2 [b]	0.1497	0.1886	0.0813	0.1318	0.0928	0.0727	0.1339

[a] $R1 = \Sigma||F_o| - |F_c||/\Sigma|F_o|$. [b] $wR2 = \{\Sigma[w(F_o^2 - F_c^2)^2]/\Sigma w(F_o^2)^2]\}^{1/2}$.

Fig. 2 (a) A view of the bridging by tpytrz ligands of a Co(II) site to the six-coordinate Mo(IV) centers of two adjacent layers. A consequence of this bonding mode is to terminate the Mo/M′/ligand chain at this trinuclear grouping; that is, the $[M'(tpytrz)_2Mo_4O_{13}]$ family does not exhibit $\{M'(ligand)\}_n$ infinite chains as substructural motifs. (b) The heterocyclic unit which links adjacent chains in $[Co(tpytrz)_2Mo_4O_{13}]$.

tetrahedral Mo site on each of two adjacent ribbons. One consequence of this connectivity pattern is to generate three distinct ring motifs within the layer: $\{CoMo_3O_4\}$, $\{Co_2Mo_4O_6\}$, and $\{Mo_4O_4\}$.

Each tetrahedral Mo site participates in bridging to two Mo octahedra of the ribbon and to a Co(II) center, leaving one terminal oxo-group. The six-coordinate molybdenum centers participate in oxo-bridges to two tetrahedral sites and one octahedral site of the ribbon and to a Co(II) unit in the equatorial plane. The axial positions are occupied by a terminal oxo-group and the nitrogen donor of a tpytrz ligand. The bimetallic oxide layer is also characterized by the presence of a stepped chain of three corner-sharing octahedra, linked through molybdenum tetrahedra. Embedded trinuclear motifs of this type are common in the structural chemistry of inorganic oxides and have been described for materials including oxovanadium phosphates,[50] oxovanadium phosphonates,[51] and metal bronzes.[52]

The tripyridyltriazine ligand functions as a bridging bidentate ligand. Thus, one arm of the ligand is pendant and participates in π-stacking in the interlamellar region. Curiously, each tpytrz ligand coordinates to a cobalt site in one layer and a molybdenum site on an adjacent layer. While nitrogen donor coordination for molybdenum-oxo species is not uncommon in both molecular and extended structures, this is an unusual bonding mode for the Mo/O/M′/ligand family of materials, as in all other instances where the polytopic, bridging ligand is not tpytrz, the nitrogen donors are associated exclusively with the secondary metal sites.

This ligation mode produces some unusual structural consequences, shown in Fig. 2. A secondary metal–ligand {Co(tpytrz)$_2$} subunit links a given oxide layer to two adjacent layers by bridging to an octahedral Mo site. Consequently, the direct metal–tpytrz chain, {Mo–tpytrz–M′–tpytrz–Mo} terminates at the Mo polyhedra and spans three layers only. Extension to the infinite metal–ligand chain requires bridging to the adjacent M′ at each molybdenum terminus of the {Mo–tpytrz–M′–tpytrz–Mo} subunit to produce the {tpytrz–M′–O–

Table 2 Selected bond lengths [Å] and angles [°] for $[Fe(tpytrz)_2Mo_4O_{13}]$ (**1**), $[Co(tpytrz)_2Mo_4O_{13}]$ (**2**), $[Ni(tpytrz)_2Mo_4O_{13}]$ (**3**), and $[Zn(tpytrz)_2Mo_3O_{13}]$ (**4**)

$[M(tpytrz)_2Mo_4O_{13}]$	**1** (M = Fe)	**2** (M = Co)	**3** (M = Ni)	**4** (M = Zn)
Mo1–O1	1.761(3)	1.752(6)	1.751(2)	1.737(5)
Mo1–O2	1.825(3)	1.824(6)	1.828(2)	1.835(4)
Mo1–O3	1.712(3)	1.716(6)	1.712(3)	1.707(5)
Mo1–O4	1.792(3)	1.802(6)	1.795(2)	1.785(4)
Mo2–O5	1.8949(4)	1.8927(6)	1.8927(6)	1.8878(6)
Mo2–O6	1.732(3)	1.735(6)	1.734(2)	1.741(4)
Mo2–O7	1.698(3)	1.704(6)	1.701(3)	1.702(5)
Mo2–O2	2.004(3)	1.999(6)	1.992(2)	1.983(5)
Mo2–O4	2.149(3)	2.141(6)	2.141(2)	2.161(5)
Mo2–N2	2.469(4)	2.462(7)	2.467(3)	2.470(5)
M–O1	2.069(3)	2.064(6)	2.050(2)	2.107(5)
M–O6	2.146(3)	2.126(6)	2.088(2)	2.174(4)
M–N2	2.198(4)	2.139(7)	2.096(3)	2.132(5)
Mo1–O1–M	152.6(2)	152.9(3)	153.1(2)	151.2(3)
Mo2–O6–M	168.5(2)	168.5(4)	170.1(1)	167.5(3)

Table 3 Selected bond lengths [Å] and angles [°] for $[Ni(H_2O)_4(Htpytrz)_2][Mo_8O_{26}]\cdot 1.2H_2O$ (**5**·$1.2H_2O$)[a]

Ni(1)–O(14)	2.055(4)
Ni(1)–O(15)#1	2.085(4)
Ni(1)–O(15)	2.085(4)
Ni(1)–N(2)	2.093(5)
Mo(1)–O(8)	1.704(4)
Mo(1)–O(10)	1.713(4)
Mo(1)–O(7)	1.905(4)
Mo(1)–O(11)	1.983(4)
Mo(1)–O(1)	2.265(4)
Mo(1)–O(9)	2.356(4)
Mo(2)–O(12)	1.693(4)
Mo(2)–O(13)	1.750(4)
Mo(2)–O(9)#2	1.949(4)
Mo(2)–O(11)	1.957(4)
Mo(2)–O(1)	2.145(4)
Mo(2)–O(1)#2	2.356(4)
Mo(3)–O(3)	1.701(4)
Mo(3)–O(2)	1.704(4)
Mo(3)–O(4)	1.901(4)
Mo(3)–O(9)#2	1.992(4)
Mo(3)–O(11)#2	2.324(4)
Mo(3)–O(1)	2.388(4)
Mo(4)–O(6)	1.687(4)
Mo(4)–O(5)	1.727(4)
Mo(4)–O(4)	1.915(4)
Mo(4)–O(7)	1.944(4)
Mo(4)–O(13)#2	2.268(4)
Mo(4)–O(1)	2.442(4)
O(14)#1–Ni(1)–O(14)	180.0(2)
O(14)–Ni(1)–O(15)#1	87.4(2)
O(14)–Ni(1)–O(15)	92.6(2)
O(15)#1–Ni(1)–O(15)	180.0(1)
O(14)–Ni(1)–N(2)#1	89.6(2)
O(15)#1–Ni(1)–N(2)#1	89.3(2)
O(15)–Ni(1)–N(2)#1	90.7(2)
O(14)–Ni(1)–N(2)	90.4(2)
O(15)–Ni(1)–N(2)	89.3(2)
N(2)#1–Ni(1)–N(2)	180.0(2)

[a] Symmetry transformations used to generate equivalent atoms: #1 $-x + 3/2, -y + 1/2, -z + 1$; #2 $-x + 1/2, -y + 3/2, -z$.

Table 4 Selected bond lengths [Å] and angles [°] for $[Ni(tpytrz)Mo_2O_7]$ (**6**)[a]

Ni(1)–O(3)#1	2.027(2)
Ni(1)–O(1)	2.053(2)
Ni(1)–N(1)	2.090(3)
Mo(1)–O(2)	1.698(3)
Mo(1)–O(1)	1.736(2)
Mo(1)–O(3)	1.741(2)
Mo(1)–O(4)	1.8694(3)
O(3)#1–Ni(1)–O(1)	90.96(9)
O(3)#2–Ni(1)–O(1)	89.04(9)
O(1)#3–Ni(1)–O(1)	180.0(1)
O(3)#1–Ni(1)–N(1)	91.33(9)
O(3)#2–Ni(1)–N(1)	88.67(9)
O(1)–Ni(1)–N(1)	92.97(9)
O(1)–Ni(1)–N(1)#3	87.03(9)
N(1)–Ni(1)–N(1)#3	180.000(1)
O(2)–Mo(1)–O(1)	109.3(1)
O(2)–Mo(1)–O(3)	109.2(1)
O(1)–Mo(1)–O(3)	109.9(1)
O(2)–Mo(1)–O(4)	111.2(1)
O(1)–Mo(1)–O(4)	107.57(8)
O(3)–Mo(1)–O(4)	109.74(7)
Mo(1)–O(1)–Ni(1)	150.4(1)
Mo(1)–O(3)–Ni(1)#4	154.7(1)
Mo(1)#5–O(4)–Mo(1)	180.0

[a] Symmetry transformations used to generate equivalent atoms: #1 $-x + 1/2, -y + 1, z + 1/2$; #2 $x + 1/2, y, -z + 3/2$; #3 $-x + 1, -y + 1, -z + 2$; #4 $-x + 1/2, -y + 1, z - 1/2$; #5 $-x, -y + 1, -z + 2$; #6 $x, -y + 3/2, z$.

Mo–tpytrz–M′–tpytrz–Mo–O–M′–tpytrz} stepped ribbon. This structural motif contrasts with the more common structural characteristic of {M′–ligand–M′} infinite chains, which are found in phases such as $[Cu(dpe)MoO_4]$. This coordination mode also serves to generate a heterocyclic structure constructed from two ligands and two binuclear $\{Co(N_2O_4)Mo(O_5N)\}$ units.

The metrical parameters for **1**–**4** and the isomorphous $[Cu(tpytrz)Mo_4O_{13}]$ are summarized in Table 2. The anticipated trend of bond length contraction is observed for Fe, Co, and Ni, while the Cu(II) structure exhibits a highly distorted '4 + 2' structure as a consequence of the Jahn–Teller effect associated with the d^9 electronic configuration.

As noted previously, a second material of the Mo/O/Ni(II)/tpytrz family is obtained at higher temperature, namely $[Ni(H_2O)_4(Htpytrz)_2][Mo_8O_{26}]\cdot 1.2H_2O$ (**5**·$1.2H_2O$). As shown in Fig. 3, the structure of **5** consists of discrete molecular $\{Ni(H_2O)_4(Htpytrz)_2\}^{4+}$ cations and $\{Mo_8O_{26}\}^{4-}$ cluster anions. The octamolybdate is the common β-cluster, constructed of edge-sharing Mo(VI) octahedra.[53] Valence sum calculations[54] and inspection of the Mo–O bond distances establish that the β-cluster is unexceptional and contains no protonated oxo-groups. Charge balance considerations require the protonation of two sites, most likely the pyridyl nitrogen positions of the monodentate tpytrz ligands.

When the reaction of $NiCl_2\cdot 6H_2O$, MoO_3 and tpytrz is carried out in the absence of base, $[Ni(tpytrz)Mo_2O_7]$ (**6**) is obtained. As shown in Fig. 4, the structure of **6** exhibits the common alternating pattern of oxide layers and buttressing organic domains. The two-dimensional oxide sheet is constructed from corner-sharing $\{NiO_4N_2\}$ octahedra and Mo(VI)

Table 5 Selected bond lengths [Å] and angles [°] for $[Zn_2(tpytrz)Mo_2O_8]$ (**7**)[a]

Zn(1)–O(3)#1	1.941(4)
Zn(1)–O(1)#2	1.953(4)
Zn(1)–N(1)	2.042(5)
Zn(1)–O(4)	2.070(4)
Zn(1)–O(1)#3	2.221(4)
Mo(1)–O(2)	1.711(5)
Mo(1)–O(3)	1.753(4)
Mo(1)–O(4)	1.755(4)
Mo(1)–O(1)	1.818(4)
O(3)#1–Zn(1)–O(1)#2	114.5(2)
O(3)#1–Zn(1)–N(1)	121.8(2)
O(1)#2–Zn(1)–N(1)	122.3(2)
O(3)#1–Zn(1)–O(4)	96.6(2)
O(1)#2–Zn(1)–O(4)	97.3(2)
N(1)–Zn(1)–O(4)	88.7(2)
O(3)#1–Zn(1)–O(1)#3	86.7(2)
O(1)#2–Zn(1)–O(1)#3	82.2(2)
N(1)–Zn(1)–O(1)#3	88.7(2)
O(4)–Zn(1)–O(1)#3	176.5(1)
O(2)–Mo(1)–O(3)	109.7(3)
O(2)–Mo(1)–O(4)	108.1(2)
O(3)–Mo(1)–O(4)	109.6(2)
O(2)–Mo(1)–O(1)	107.9(2)
O(3)–Mo(1)–O(1)	111.5(2)
O(4)–Mo(1)–O(1)	109.9(2)
Mo(1)–O(1)–Zn(1)#2	133.5(2)
Mo(1)–O(1)–Zn(1)#5	126.8(2)
Zn(1)#2–O(1)–Zn(1)#5	97.8(2)
Mo(1)–O(3)–Zn(1)#6	161.9(3)
Mo(1)–O(4)–Zn(1)	148.4(2)

[a] Symmetry transformations used to generate equivalent atoms: #1 $x + 1/2, y, -z + 1/2$; #2 $-x, -y + 1, -z + 1$; #3 $x + 1, y, z$; #4 $-x + 1, -y + 1, -z + 1$; #5 $x - 1, y, z$; #6 $x - 1/2, y, -z + 1/2$; #7 $x, -y + 1/2, z$.

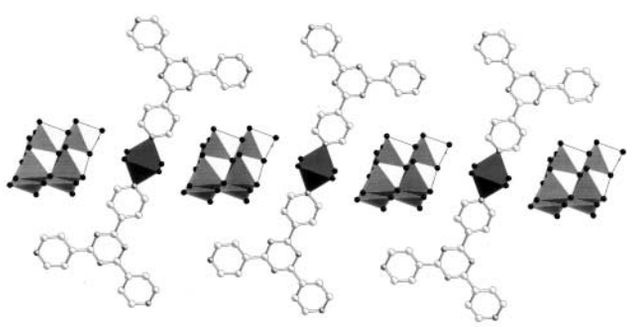

Fig. 3 A view of the β-$[Mo_8O_{26}]^{4-}$ clusters and the $[Ni(H_2O)_4(Htpytrz)_2]^{4+}$ cations of **5**·1.2H_2O.

tetrahedra. The molybdenum oxide subunit is present as $\{Mo_2O_7\}$ or dimolybdate clusters. Each dimolybdate moiety is linked to four adjacent $\{NiO_4N_2\}$ octahedra, and each Ni site bridges four neighboring dimolybdate subunits. Consequently, the bimetallic oxide substructure $\{NiMo_2O_7\}$ may be described in terms of the fusing of heterocyclic $\{Ni_2Mo_3O_5\}$ ten-membered rings.

The geometry at the Ni(II) sites is defined by four oxo-groups from four dimolybdate units in the equatorial plane and two nitrogen donors from tpytrz ligands in the axial positions. Thus, each Ni(II) octahedron is bridged to Ni sites on each of two neighboring layers by the tpytrz ligands which project into the interlamellar region. In common with structures **1**–**4**, one arm of each tpytrz ligand is pendant and serves a space-filling role in the interlamellar domain. A secondary structural motif is provided by $\{Ni(tpytrz)\}_n^{2n+}$ chains which serve to link the bimetallic oxide sheets into an overall three-dimensional covalent framework.

It is noteworthy that compound **6** contains the $\{Mo_2O_7\}^{2-}$ subunit embedded within the bimetallic oxide substructure. The $\{Mo_2O_7\}^{2-}$ unit is a common molecular species,[55] and

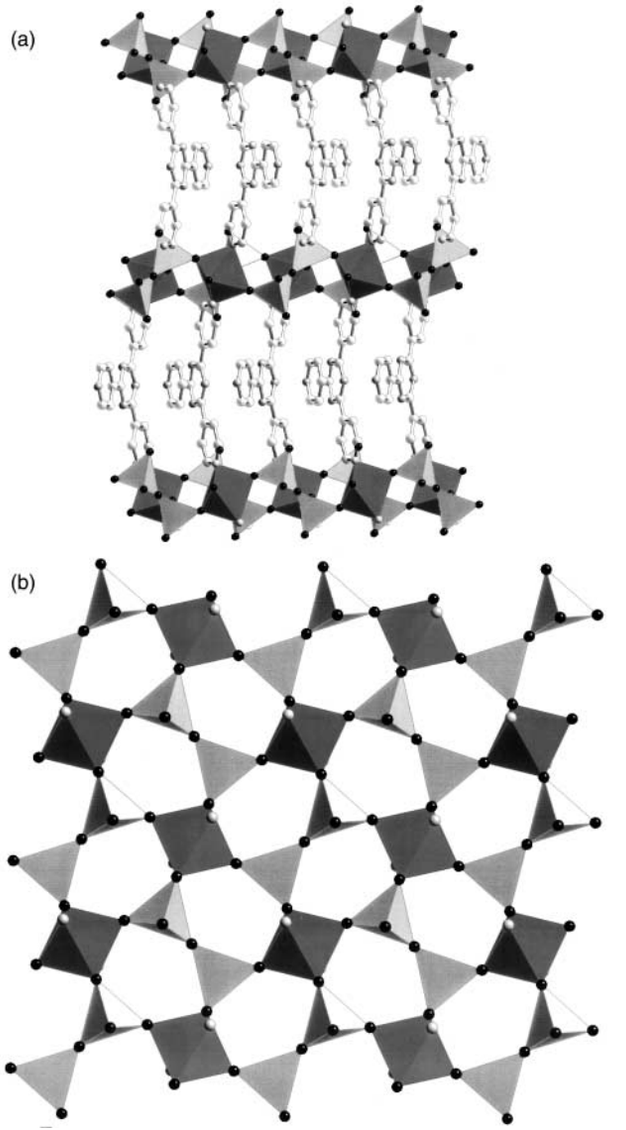

Fig. 4 (a) A view of the layer stacking for $[Ni(tpytrz)Mo_2O_7]$ (**6**). (b) A view of the bimetallic oxide network.

the structurally analogous unit $\{V_2O_7\}^{4-}$ may be found as a substructural motif of some oxide materials.[56] However, in surveying the structures of the family of materials of the type Mo/O/M′/organonitrogen ligand, three molybdenum oxide building blocks are commonly observed: $\{MoO_4\}^{2-}$ tetrahedra, octamolybdate clusters and one-dimensional molybdate chains. Compound **6** is a unique example of a material of this class exhibiting the $\{Mo_2O_7\}^{2-}$ subunit. The divanadate subunit $\{V_2O_7\}^{4-}$ is similarly an unusual structural motif in the V/O/M′/ligand family and to date has been observed only in $(H_2en)[Mn_3(H_2O)_2V_4O_{14}]$.[38e]

Reaction conditions also affect the hydrothermal chemistry of the Mo/O/Zn/tpytrz phases. Thus, under basic conditions, $[Zn_2(tpytrz)Mo_2O_8]$ (**7**) is isolated as large orange crystals. As shown in Fig. 5, the structure of **7** again exhibits the alternation of bimetallic oxide sheets and organic interlamellar domains.

The $\{ZnMoO_4\}$ layers are constructed from $\{MoO_4\}$ tetrahedra and five-coordinate $\{ZnO_4N\}$ sites. The zinc sites are present as edge-sharing binuclear units. The distorted five-coordinate geometry at the Zn(II) site is defined by four oxo-groups from four $\{MoO_4\}$ tetrahedra and the nitrogen donor of a tpytrz ligand. One polyhedral edge of the Zn site is shared with an adjacent Zn polyhedron to form a binuclear unit. Each $\{MoO_4\}$ tetrahedron links to three binuclear Zn sites, leaving one terminal oxo-group which projects into the interlamellar region. Two of the oxo-groups adopt the μ^2-bridging mode

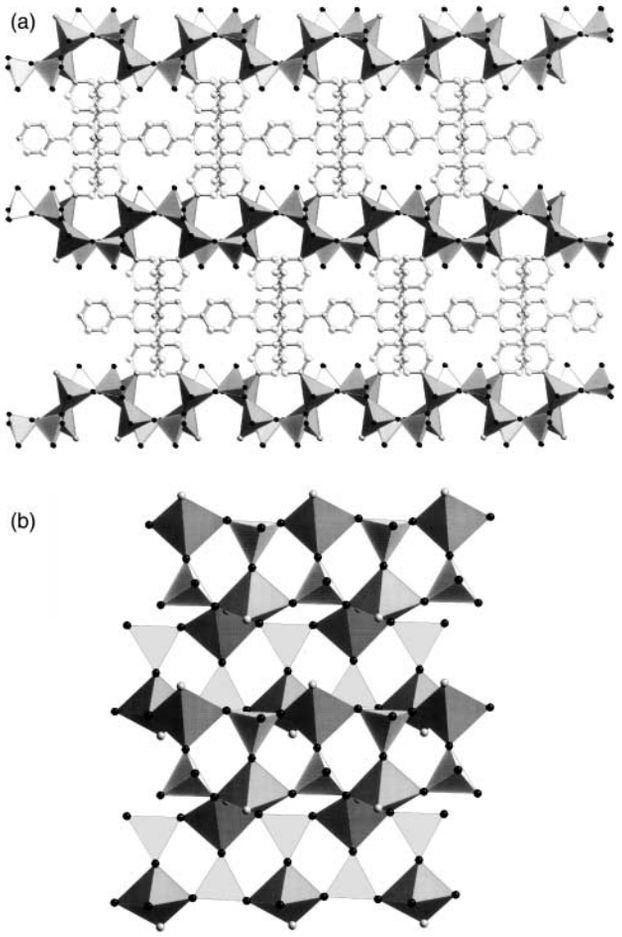

Fig. 5 (a) A view of the layer stacking for $[Zn_2(tpytrz)Mo_2O_8]$ (**7**), showing the sinusoidal profile of the oxide layers. (b) A view of the bimetallic oxide network.

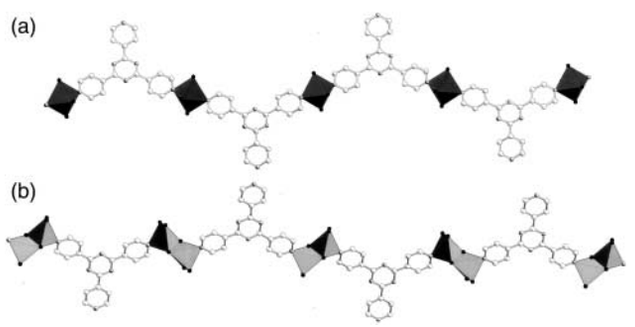

Fig. 6 (a) The one-dimensional $\{Ni(tpytrz)\}_n^{+2n}$ chain of **6**. (b) The one-dimensional $\{Zn_2(tpytrz)\}_n^{+4n}$ chain of **7**.

{Mo–O–Zn}, while the third exhibits μ^3-bridging $\{MoZn_2O\}$. One consequence of this connectivity pattern is to produce a distinctive sinusoidal ruffling to the bimetallic oxide layer with period of *ca.* 10.3 Å and amplitude 6.2 Å. This is reminiscent of the structure of $[\{Zn(bpy)_2\}_2V_6O_{17}]$.[13]

Another curious feature of the structure of **7** is the presence of a novel one-dimensional $\{Zn_2(tpytrz)\}$ chain substructure, shown in Fig. 6. Unlike the more common one-dimensional M′–ligand motifs which consist of M′ polyhedra linked to two *trans* disposed bridging ligands, as encountered for **6**, the one-dimensional substructure of **7** exhibits a binuclear zinc unit with one tpytrz ligand projecting from each metal site.

The occurrence of pendant pyridyl arms in the structures of **1**–**4**, **6**, and **7** is reflected in their thermal characteristics. For example, as shown in Fig. 7 for $[Ni(tpytrz)_2Mo_4O_{13}]$, the thermal decomposition exhibits a weight loss of *ca.* 12% between 300–350 °C, consistent with the loss of a pyridyl group.

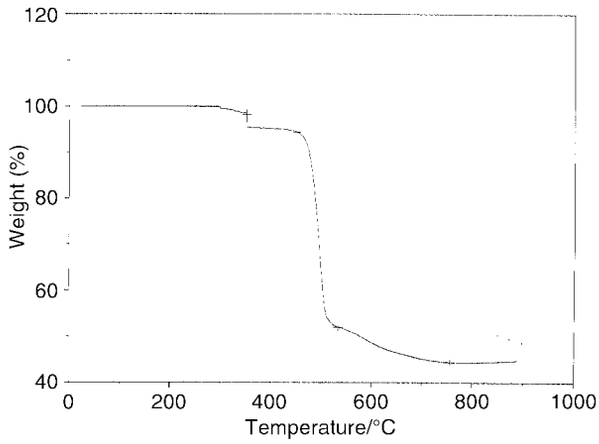

Fig. 7 Thermogravimetric curve for the thermal decomposition of $[Ni(tpytrz)_2Mo_4O_{13}]$.

This conclusion is supported by elemental analyses of the products of heating of **3** and **6** at 350 °C in dynamic vacuum for 2 h, which were consistent with the loss of a pyridyl unit. This thermal product for **3** is stable to 450 °C, whereupon a second weight loss of 40% occurs, corresponding to the loss of the bipyridyltriazine ligand fragment. The resultant gray residue is amorphous.

Conclusions

Advances in the chemistry of materials are driven by synthesis and the discovery of novel compositions and structures. A powerful strategy for the development of new materials combines hydrothermal techniques with the introduction of organic components as structure-directing subunits in the construction of organic–inorganic composites. In the specific case of molybdenum oxide based materials, organonitrogen ligands may be exploited to modify the oxide microstructure. In this fashion, a series of bimetallic oxide layers buttressed by tripyridyltriazine ligands acting as dipodal bridges has been prepared and structurally characterized. The compounds **1**–**4**, **6**, and **7** exhibit the characteristic architecture of alternating inorganic oxide networks and tethering ligand domains, in the construction of a material of overall three-dimensional covalent connectivity. However, significant variations in network structure are observed as a consequence of modifications in reaction conditions of temperature and/or pH. Similarly, comparison of the structures of this study to those of other members of the Mo/O/M′/ligand family such as $[Cu(dpe)MoO_4]$, $[Cu(bpa)_{0.5}MoO_4]$, and $[\{Ni(3,3'\text{-bpy})_2\}_2Mo_4O_{14}]$, reveals that variations in ligand geometry also produce profound changes in the oxide microstructures.

The hydrothermal method overcomes the limitation of being able to synthesize only the thermodynamic dense phases obtained by classical ceramic methods and provides an approach to the design of zeolites and other microporous solids, high-T_c cuprates, intercalation compounds, pillared layered materials and in our case inorganic–organic hybrid materials, all of which may be considered metastable materials.

Thus, the synthetic approach adopted for the evolution of these oxide hybrid materials draws on the fundamental principles of coordination chemistry in their design. The guiding principle in this strategy is that the information necessary for the design of the extended hybrid structures is present at the molecular level in the starting materials or component building blocks. Consequently the syntheses rely on self-assembly and borrow conceptually from the fields of supramolecular chemistry and "crystal engineering".[57] However, it is important to appreciate that the design principles inherent in this approach provide only a broad blueprint, relying often on serendipitous discovery of new architectures and the judicious

selection of component substructures.[58] While the ability to rationally design materials for use in fundamental studies or practical applications motivates such synthetic studies, the complexity and range of interactions within most solids precludes accurate structural predictions. However, through the accumulation of a structural database for a particular family of materials, empirical rules can emerge to aid in the design and control of structure.

Acknowledgements

This work was supported by a grant from the National Science Foundation (CHE9987471).

References

1 N. N. Greenwood and A. Earnshaw, *Chemistry of the Elements*, Pergamon Press, New York, 1984.
2 (*a*) W. Büchner, R. Schiebs, G. Winter and K. H. Büchel, *Industrial Inorganic Chemistry*, VCH, New York, 1989; (*b*) B. Cockayne and D. W. Jones, *Modern Oxide Materials*, ed. D. W. Jones, Academic Press, New York, 1972.
3 C. R. Kagan, D. B. Mitzi and C. D. Dimitrakopoulos, *Science*, 1999, **286**, 945.
4 (*a*) D. B. Mitzi, *J. Chem. Soc., Dalton Trans.*, 2001, 1; (*b*) D. B. Mitzi, *Inorg. Chem.*, 2000, **39**, 6107.
5 (*a*) S. I. Stupp and P. V. Braun, *Science*, 1997, **277**, 1242; (*b*) M. E. Davis, A. Katz and W. R. Ahmad, *Chem. Mater.*, 1996, **8**, 1820.
6 (*a*) J. M. Newsam, in *Solid State Chemistry: Compounds*, ed. A. K. Cheetham and P. Day, Clarendon Press, Oxford, 1992, vol. 234; (*b*) J. A. Raleo, *ACS Monogr.*, 1976, **7**; (*c*) *New Development in Zeolite Science*, ed. Y. Murakami, A. Iijima and J. W. Ward, Elsevier, Amsterdam, 1986; (*d*) D. E. W. Vaughan, *Spec. Publ.-Chem. Soc.*, 1979, **33**, 294; (*e*) P. B. Venuto, *Microporous Mater.*, 1994, **2**, 297; (*f*) R. Szostak, *Molecular Sieves—Principles of Synthesis and Identification*, Van Nostrand Rheinhold, New York, 2nd edn., 1997.
7 C. T. Kresge, M. E. Leonowicz, W. J. Roth, J. C. Vartuli and J. S. Beck, *Nature*, 1992, **359**, 710.
8 (*a*) R. C. Haushalter and L. A. Mundi, *Chem. Mater.*, 1992, **4**, 31; (*b*) M. L. Khan, L. M. Meyer, R. C. Haushalter, C. L. Schweitzer, J. Zubieta and J. L. Dye, *Chem. Mater.*, 1996, **8**, 43.
9 (*a*) S. Ayyappan, G. Diaz de Delgado, A. K. Cheetham, G. Férey and C. N. R. Rao, *J. Chem. Soc., Dalton Trans.*, 1999, 2905 and references therein; (*b*) C. V. K. Sharma and A. Clearfield, *J. Am. Chem. Soc.*, 2000, **122**, 1558; (*c*) R. C. Finn and J. Zubieta, *J. Chem. Soc., Dalton Trans.*, 2000, 1821 and references therein.
10 R. C. Finn and J. Zubieta, *Prog. Inorg. Chem.*, in press.
11 P. J. Hagrman, R. L. LaDuca, Jr., H.-J. Koo, R. S. Rarig, Jr., R. C. Haushalter, M.-H. Whangbo and J. Zubieta, *Inorg. Chem.*, 2000, **39**, 4311.
12 P. J. Hagrman and J. Zubieta, *Inorg. Chem.*, 2000, **39**, 3252.
13 Y. Zhang, J. R. D. DeBord, C. J. O'Connor, R. C. Haushalter, A. Clearfield and J. Zubieta, *Angew. Chem., Int. Ed. Engl.*, 1996, **35**, 989.
14 J. R. D. DeBord, Y. Zhang, R. C. Haushalter, J. Zubieta and C. J. O'Connor, *J. Solid State Chem.*, 1996, **122**, 251.
15 R. L. LaDuca, Jr., R. C. Finn and J. Zubieta, *Chem. Commun.*, 1999, 1669.
16 R. L. LaDuca, Jr., R. S. Rarig, Jr. and J. Zubieta, *Inorg. Chem.*, 2001, **40**, 607.
17 P. J. Ollivier, J. R. D. DeBord, P. J. Zapf, J. Zubieta, L. M. Meyer, C.-C. Wang, T. E. Mallouk and R. C. Haushalter, *J. Mol. Struct.*, 1998, **470**, 49.
18 P. J. Hagrman, C. Bridges, J. E. Greedan and J. Zubieta, *J. Chem. Soc., Dalton Trans.*, 1999, 2901.
19 R. C. LaDuca, Jr., C. Brodkin, R. C. Finn and J. Zubieta, *Inorg. Chem. Commun.*, 2000, **3**, 248.
20 P. J. Hagrman, D. Hagrman and J. Zubieta, *Angew. Chem., Int. Ed.*, 1999, **38**, 2638.
21 D. Hagrman, C. Zubieta, R. C. Haushalter and J. Zubieta, *Angew. Chem., Int. Ed. Engl.*, 1997, **36**, 873.
22 D. Hagrman, C. Sangregorio, C. J. O'Connor and J. Zubieta, *J. Chem. Soc., Dalton Trans.*, 1998, 3707.
23 D. Hagrman, P. Hagrman and J. Zubieta, *Inorg. Chim. Acta*, 2000, **300–302**, 212.
24 J. R. D. DeBord, R. C. Haushalter, L. M. Meyer, D. J. Rose, P. J. Zapf and J. Zubieta, *Inorg. Chim. Acta*, 1997, **256**, 165.
25 D. Hagrman, P. J. Zapf and J. Zubieta, *Chem. Commun.*, 1998, 1283.
26 D. Hagrman, P. J. Hagrman and J. Zubieta, *Angew. Chem., Int. Ed.*, 1999, **38**, 3165.
27 D. Hagrman and J. Zubieta, *C. R. Acad. Sci., Ser. IIc*, 2000, **3**, 231.
28 D. Hagrman, P. J. Hagrman and J. Zubieta, *Comments Inorg. Chem.*, 1999, **21**, 225 and references therein.
29 D. J. Chesnut, D. Hagrman, P. J. Zapf, R. P. Hammond, R. LaDuca, Jr., R. C. Haushalter and J. Zubieta, *Coord. Chem. Rev.*, 1999, **190–192**, 737.
30 P. J. Zapf, R. P. Hammond, R. C. Haushalter and J. Zubieta, *Chem. Mater.*, 1998, **10**, 1366.
31 D. Hagrman, C. J. Warren, R. C. Haushalter, C. Seip, C. J. O'Connor, R. S. Rarig, Jr., K. M. Johnson III, R. L. LaDuca, Jr. and J. Zubieta, *Chem. Mater.*, 1998, **10**, 3294.
32 D. Hagrman, R. C. Haushalter and J. Zubieta, *Chem. Mater.*, 1998, **10**, 361.
33 M. C. Laskoski, R. L. LaDuca, Jr., R. S. Rarig, Jr. and J. Zubieta, *J. Chem. Soc., Dalton Trans.*, 1999, 3467.
34 D. E. Hagrman and J. Zubieta, *J. Solid State Chem.*, 2000, **152**, 141.
35 R. L. LaDuca, Jr., M. Desciak, M. Laskoski, R. S. Rarig, Jr. and J. Zubieta, *J. Chem. Soc., Dalton Trans.*, 2000, 2255.
36 P. J. Zapf, C. J. Warren, R. C. Haushalter and J. Zubieta, *Chem. Commun.*, 1997, 1543.
37 S. Aschwanden, H. W. Schmalle, A. Reller and H. R. Oswald, *Mater. Res. Bull.*, 1993, **28**, 45.
38 For other examples of the V/O/M′/ligand family, see also (*a*) B.-Z. Lin and S.-X. Liu, *Polyhedron*, 2000, **19**, 2521; (*b*) L.-M. Zheng, J.-S. Zhao, K.-H. Lii, L.-Y. Zhang, Y. Liu and X.-Q. Xin, *J. Chem. Soc., Dalton Trans.*, 1999, 939; (*c*) R. Chen, P. Y. Zavalij, M. S. Whittingham, J. E. Greedan, N. P. Raju and M. Bieringer, *J. Mater. Chem.*, 1999, 93; (*d*) Z. Shi, L. Zhang, G. Zhu, G. Yang, J. Hua, H. Ding and S. Feng, *Chem. Mater.*, 1999, **11**, 3565; (*e*) T. S.-C. Law and I. D. Williams, *Chem. Mater.*, 2000, **12**, 2070; (*f*) L.-M. Zheng, T. Whitfield, X. Wang and A. J. Jacobson, *Angew. Chem., Int. Ed.*, 2000, **39**, 4528.
39 H. G. Biedermann and K. Wichmann, *Z. Naturforsch.*, 1974, **296**, 360.
40 SMART, Data Collection Software, version 4.050, Siemens Analytical Instruments Inc., Madison, WI, 1996.
41 SAINT, Data Reduction Software, version 4.050, Siemens Analytical Instruments Inc., Madison, WI, 1996.
42 G. M. Sheldrick, SADABS, University of Göttingen, 1996.
43 SHELXTL PC, Siemens Analytical X-Ray Instruments Inc., Madison, WI, 1993.
44 R. A. Laudise, *Chem. Eng. News*, 1987, **65**, 30.
45 A. N. Lobachev, *Crystallization Processes Under Hydrothermal Conditions*, Consultants Bureau, New York, 1973.
46 J. Gopalakrishnan, *Chem. Mater.*, 1995, **7**, 1265.
47 R. Chen, P. Y. Zavalij, M. S. Whittingham, J. E. Greedan, N. P. Raju and M. Bieringer, *J. Mater. Chem.*, 1999, **9**, 93.
48 (*a*) A. Clearfield, *Prog. Inorg. Chem.*, 1998, **47**, 371; (*b*) D. M. Poojary, B. Zhang, P. Bellinghausen and A. Clearfield, *Inorg. Chem.*, 1996, **35**, 5254; (*c*) G. Huan, A. J. Jacobson, J. W. Johnson and E. W. Corcoran, Jr., *Chem. Mater.*, 1990, **2**, 91.
49 D. B. Mitzi, *J. Chem. Soc., Dalton Trans.*, 2001, 1.
50 (*a*) A. Leclaire, J. Chardon, A. Grandin, M. M. Borel and B. Raveau, *J. Solid State Chem.*, 1994, **108**, 291; (*b*) V. Soghomonian, Q. Chen, R. C. Haushalter, J. Zubieta, C. J. O'Connor and Y.-S. Lee, *Chem. Mater.*, 1993, **5**, 1690.
51 (*a*) G. Bonavia, R. C. Haushalter, C. J. O'Connor and J. Zubieta, *Inorg. Chem.*, 1996, **35**, 5603; (*b*) M. I. Khan, Y.-S. Lee, C. J. O'Connor, R. S. Haushalter and J. Zubieta, *Inorg. Chem.*, 1994, **33**, 3850.
52 (*a*) M. Greenblatt, *NATO ASI Ser., Ser. C*, 1996, **354**, 15; (*b*) M. Greenblatt, *Chem. Rev.*, 1988, **88**, 31.
53 M. T. Pope, *Heteropoly and Isopoly Oxometalates*, Springer, New York, 1983.
54 I. D. Brown and K. K. Wu, *Acta Crystallogr., Sect. B*, 1976, **32**, 1957.
55 V. W. Day, M. F. Fredrick, W. G. Klemperer and W. Shum, *J. Am. Chem. Soc.*, 1977, **99**, 6146.
56 (*a*) I. D. Williams, T. S.-C. Law, H. H.-Y Sung, G.-H. Wen and X.-X. Zhang, *Solid State Sci*, 2000, **2**, 47; (*b*) Y. Zhang, J. R. D. DeBord, C. J. O'Connor, R. C. Haushalter, A. Clearfield and J. Zubieta, *Angew. Chem., Int. Ed. Engl.*, 1996, **35**, 989; (*c*) J. R. D. DeBord, Y. Zhang, R. C. Haushalter, J. Zubieta and C. J. O'Connor, *J. Solid State Chem.*, 1996, **122**, 251.
57 "Crystal engineering" is here used in the broadest sense of modification of the extended structure of a material. The organic components in the hybrid materials of this study allow isolation of bimetallic oxide chains which are otherwise inaccessible in the M(II)/Mo/O solid state chemistry.
58 M. J. Zaworotko, *Chem. Commun.*, 2001, 1.